Correspondence and
requests for materials
should be addressed to
G.K. (gkoren@physics.
technion.ac.il)

Pairing and the phase diagram of the normal coherence length $\xi_N(T, x)$ above T_c of $La_{2-x}Sr_xCuO_4$ thin films probed by the Josephson effect

Tal Kirzhner & Gad Koren

Physics Department, Technion-Israel Institute of Technology, Haifa 32000, Israel.

The long range proximity effect in high-T_c c-axis Josephson junctions with a high-T_c barrier of lower T_c is still a puzzling phenomenon. It leads to supercurrents in junctions with much thicker barriers than would be allowed by the conventional proximity effect. Here we measured the $T - x$ (Temperature-doping level) phase diagram of the barrier coherence length $\xi_N(T, x)$, and found an enhancement of ξ_N at moderate under-doping and high temperatures. This indicates that a possible origin of the long range proximity effect in the cuprate barrier is the conjectured pre-formed pairs in the pseudogap regime, which increase the length scale over which superconducting correlations survive in the seemingly normal barrier. In more details, we measured the supercurrents I_c of Superconducting - Normal - Superconducting SNS c-axis junctions, where S was optimally doped $Y Ba_2Cu_3O_{7-\delta}$ below T_c (90 K) and N was $La_{2-x}Sr_xCuO_4$ above its T_c (<25 K) but in the pseudogap regime. From the exponential decay of $I_c(T) \propto exp[-d/\xi_N(T)]$, where d is the barrier thickness, the $\xi_N(T)$ values were extracted. By repeating these measurements for different barrier doping levels x, the whole phase diagram of $\xi_N(T, x)$ was obtained.

A controversy still exist concerning the nature of the pseudogap regime in the cuprate superconductors[1,2]. Some researchers visualize the pseudogap regime as a precursor to superconductivity, where uncorrelated pairs which form below the pseudogap cross-over temperature T^*, acquire global phase coherence at T_c[3]. Others view the pseudogap regime as a phase or phases which are competing with superconductivity such as in spin and charge density waves and when charge, magnetic and gyrotropic orders occur[4–12]. The former group bases its case mostly on tunneling and ARPES measurements[2,13,14] of a single energy gap which evolves smoothly while crossing from the superconducting phase into the pseudogap regime. The latter group uses different observations of two distinct energy gaps, obtained by the same techniques, to rest their case[15,16]. The whole picture of the pseudogap regime however, seems to be much more complex as various experiments show precursor superconductivity coexisting with competing orders in the same samples[6,17,18]. A possible origin for the competing and coexisting orders is the inherent inhomogeneity of the surface of the cuprates, but global measurements which average over these inhomogeneities, still bring up new results which lend support to one or more of the above mentioned scenarios[19]. Polarized elastic neutron scattering and ultrasound measurements in $Y Ba_2Cu_3O_{6+x}$ have shown that the pseudogap is bound by a line of a real thermodynamic phase transition rather than by a cross over regime only[8,20]. So the controversy on the origin of the pseudogap regime is still ongoing[21].

Here we focus on properties of the pseudogap as revealed by supercurrent measurements in superconducting - normal - superconducting SNS Josephson junctions, where N is in the pseudogap regime of a cuprate barrier with a T_c lower than that of S. The observed results are closely related to the long-range (or "giant") proximity effect in trilayer c-axis junctions which was investigated previously both experimentally and theoretically[22–25]. In one of these studies, supercurrents were observed also at temperatures significantly above T_c of the N-barrier, even when its thickness was two orders of magnitude larger than the expected "normal" coherence length $\xi_N \approx 0.2$ nm for transport in the c-axis direction[22]. The actual ξ_N is therefore long ranged compared to that of the conventional proximity effect, and seems to reflect the specific nature of the pseudogap regime with its conjectured preformed pairs. To further substantiate this hypothesis, a systematic study of the supercurrent I_c dependence on temperature T and barrier doping level x is needed. This was done in the present study using $Y Ba_2Cu_3O_{7-\delta}$ —

$La_{2-x}Sr_xCuO_4 - YBa_2Cu_3O_{7-\delta}$ junctions (for $x=0.07, 0.1, 0.18$ and 0.24), with the intention of obtaining a phase diagram of $\xi_N(T, x)$ from the measured $I_c(T, x)$ data. Since the proportionality constant of the proximity relation $I_c \propto exp[-d/\xi_N]$ is unknown, we had to have $I_c(T, x)$ data for at least two different d values for each doping level x in order to extract $\xi_N(T, x)$. Once done, we present a novel phase diagram of $\xi_N(T, x)$ of $La_{2-x}Sr_xCuO_4$ above its T_c and in its pseudo-gap regime, where on the T versus x diagram, the contours of constant $\xi_N(T, x)$ for $T > 55$ K have a maximum in the underdoped regime. This provides further supporting evidence for the precursor superconductivity scenario in the cuprates.

Preparation of the junctions. We chose to work with fully epitaxial SS'S thin film junctions of the cuprates that have a conveniently wide temperature range where S' is in the pseudogap regime between the T_c values of S' and S. In this regime, we shall refer to the junctions as SNS junctions, which is the more commonly used term in such a situation. Optimally doped $YBa_2Cu_3O_{7-\delta}$ (YBCO) with $T_c \approx 90$ K was chosen as the S electrodes, while the S' barrier was chosen to be $La_{2-x}Sr_xCuO_4$ (LSCO-x) with T_c values of up to about 25 K. A schematic cross-section of a junction is shown in the top inset of Fig. 1. The trilayer film of YBCO/LSCO-x/YBCO was grown epitaxially in-situ by laser ablation deposition on 10×10 mm^2 wafers of (100) $SrTiO_3$. The trilayer was then patterned by photolithography and Ar ion milling to produce ten base electrodes with their corresponding ramps on the wafer. This was followed by a room temperature deposition of the gold cover electrode, which unlike in our previous ramp junctions[26], left the ramp of the base electrode in a highly resistive state, with only a negligible current flow in the a–b plane direction through it for the lack of the high temperature annealing step. This yielded a cross-over junction where the current flows mostly in the c-axis direction via a 5×5 μm^2 area (defined by a second patterning process) into the gold cover electrode.

Transport results. Fig. 1 shows a typical resistance versus temperature curve of a Josephson junction with a 20 nm thick $La_{1.93}Sr_{0.07}CuO_4$ barrier with 7% Sr doping (LSCO-0.07). The YBCO electrodes become superconducting at $T_c \approx 90$ K where the junction resistance drops sharply. It doesn't however drop to zero, as

can be seen in the bottom inset of Fig. 1 which shows a knee-like structure down to about 50 K on top of an almost constant residual resistance of ~ 0.3 Ω below it. These two resistance components originate in the barrier material in the junction (the LSCO-0.07 layer) and the gold cover electrode. Once the LSCO-0.07 layer becomes superconducting at about 50 K by the proximity effect, the constant residual resistance below it is due to the gold cover electrode only. Thus, as we lower the temperature further, the Josephson current increases but the series resistance of the Au cover electrode remains.

A typical I-V curve at 10 K of this type of Josephson junction is shown in Fig. 2. This curve shows that the junction has a critical current of 0.55 mA as measured by a 5 μV criterion. It also exhibits a resistively shunted junction (RSJ) behavior at higher bias with a normal resistance of 0.8 Ω. The I_cR_N product of the junction is therefore equal to 0.44 meV which is typical of Josephson junctions in the cuprates[27]. The inset of Fig. 2 depicts a conductance spectrum of this Josephson junction at 40 K under 10.7 GHz microwave irradiation, showing the AC Josephson effect. The evenly spaced peaks in the curve are due to Shapiro steps in the I-V curve at a somewhat larger than the expected spacing of $\Delta V = h\nu/2e$ due to the series resistance of about 0.3 Ω of the gold cover electrode. On a wafer with 10 junctions, the spread of the measured critical current values was about $\pm 30\%$. In the following measurements of I_c versus T on each wafer with a given barrier thickness and doping level, we had chosen to work on the junction whose critical current value is closest to the average value obtained on that wafer.

Next we focus on the temperature dependence of the critical currents which were extracted from the I-V curves using a 5 μV criterion. Fig. 3 shows the temperature dependence of the critical currents in two representative Josephson junctions with LSCO-0.07 barriers on two different wafers. One with a 20 nm thick barrier and the other with a thinner 12 nm thick barrier. At temperatures above 40–50 K, when the critical currents are small, they decay versus temperature as a $(T_c - T)^2$ power law as predicted by the De-Gennes dirty limit proximity effect formula[28]. At lower temperatures, as the supercurrents increase, the I-V curves deviate from the weak-link RSJ model and start to show a strong-link flux flow behavior which changes the power law temperature dependence. This may be
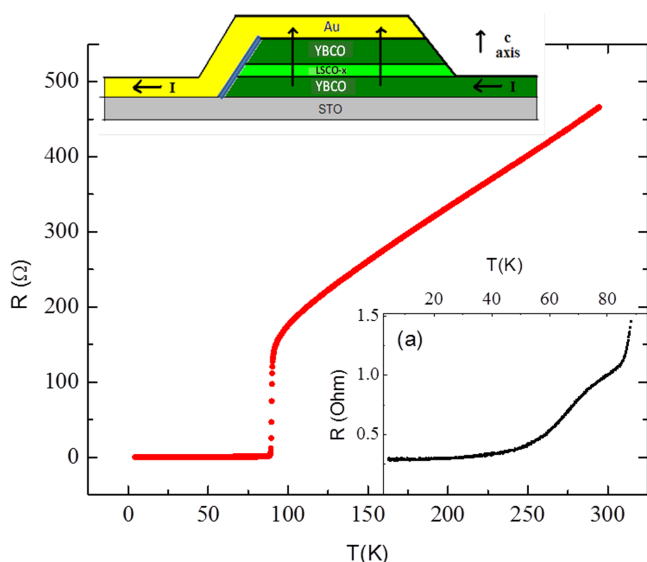

Figure 1 | Resistance versus temperature of a Josephson junction with a 20 nm thick LSCO-0.07 barrier obtained using a 100 μA current bias. The top inset shows a schematic cross-section of the junction, and the bottom one is a zoom-in on the resistance below the transition of the YBCO electrodes.
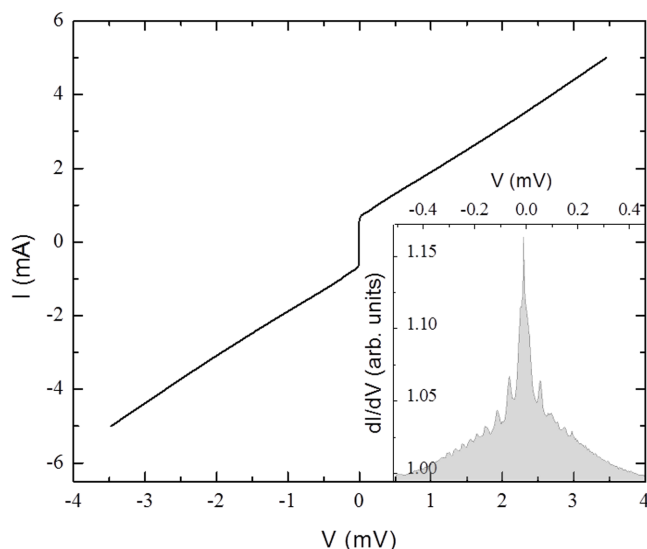

Figure 2 | Current versus voltage at 10 K of a Josephson junction with a 20 nm thick LSCO-0.07 barrier. A gold series resistance of 0.3 Ω was subtracted from the data. The inset shows the conductance of this junction at 40 K under 10.7 GHz microwave irradiation, where the Shapiro steps in the corresponding I-V curve are seen as evenly spaced peaks.
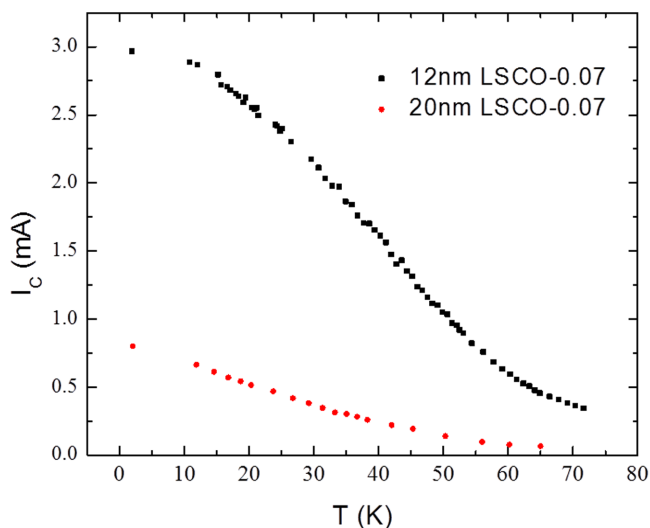
Figure 3 | Critical current as a function of temperature of two Josephson junctions on two different wafers with LSCO-0.07 barrier thicknesses of 20 nm and 12 nm.

Figure 4 | Normal coherence lengths ξ_N of LSCO-0.1 and LSCO-0.18 as a function of temperature. The inset shows the normal state resistivity of the corresponding LSCO-x barriers as a function of temperature.

due to the self field effect when the width of the junction w becomes larger than the Josephson penetration depth λ_J. A critical current of about 1.5 mA at 40 K with the 12 nm thick barrier, corresponds to a Josephson penetration depth λ_J of $\simeq 4~\mu m$ which is of the order of the width of our junctions ($w = 5~\mu m$).

Extraction of $\xi_N(T, x)$ from the data. We now turn to the main result of this study which shows the normal coherence lengths of the LSCO-x barriers at different doping levels. For any given temperature T and doping level x, the normal coherence length of the barrier can be extracted from the ratio of the critical currents in junctions with two different barrier thicknesses d_i using the exponential part of the De-Gennes formula ($I_{ci} \propto exp[-d_i/\xi_N]$[28]). To further clarify the procedure of extracting $\xi_N(T)$ from the data, a detailed description is given in the supplementary material for the case of LSCO-0.24 film and junctions. Fig. 4 shows the normal coherence lengths $\xi_N(T, x)$ for $x=0.1$ and $x=0.18$ LSCO-x barriers as a function of temperature. The temperature range of the coherence lengths plots is limited here to 40–60 K. The lower bound of the temperature range is set by the flux flow phenomenon in the junctions with the thinner barrier due to the high I_c values and rounding of the I-V curves which make the determination of I_c difficult. The upper bound is set by the low critical currents in the junctions with the thicker barrier which are noisy and therefore hard to measure. Fig. 4 shows that the measured normal coherence length values range between 4–6 nm. These values are much higher than expected from the conventional proximity effect theory[28], where the coherence length should be limited by the short c-axis superconductor coherence length ξ_S and the corresponding mean free path l_N, both of which are shorter than 1 nm. Previous experiments on SNS cuprate junctions of the type LSCO-LCO-LSCO had also shown very long coherence lengths[22]. This "giant proximity effect" was explained by a number of theories which took into account superconducting phase fluctuations above T_c in the barrier[24,25].

Discussion

Another interesting feature in Fig. 4 is the unexpected crossing of the ξ_N curves at about 55 K for the two doping levels. At low temperatures, the overdoped LSCO-0.18 barrier has a higher normal coherence length than the underdoped LSCO-0.1. This behavior however is reversed above 55 K, where the coherence length of the LSCO-0.1
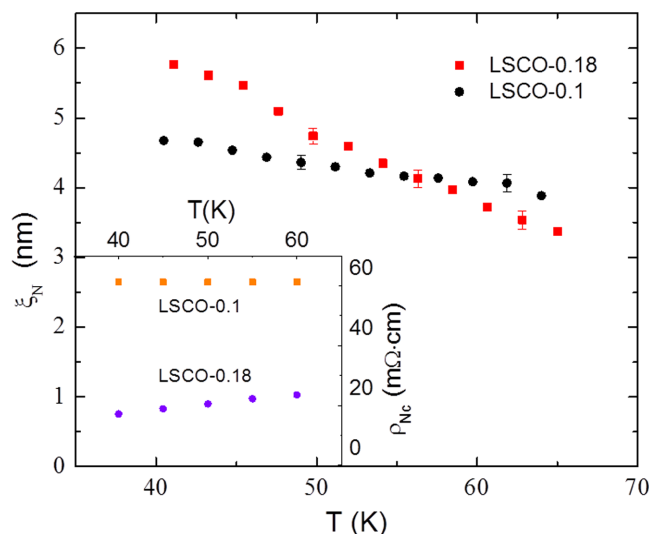
barrier becomes higher. In the following we shall try to understand this peculiar dependence of ξ_N of LSCO-x which is a dirty limit material for transport in the c-axis direction. As we shall calculate only the ratio of coherence lengths $\xi_N(0.18)/\xi_N(0.1)$, any effect of the long range proximity effect should cancel out to a first approximation. Moreover, long range proximity effect was obtained using the standard proximity effect while invoking strong superconducting "pockets" in the barrier[24], which is similar to the pre-formed pairs scenario[3]. We shall thus use here the conventional proximity effect theory. In the dirty limit this yields the normal coherence length

$$\xi_{Nd} = \sqrt{\frac{\hbar D_N}{2\pi k_B T}} \qquad (1)$$

where D_N is the diffusion constant. In order to estimate the value of D_N, we used the normal resistivity values obtained from the I-V curves of our junctions at high bias. The resulting resistivity values $\rho_{Nc}(T, x)$ are plotted in the inset of Fig. 4. In our junctions the current flows in the c-axis direction and therefore these $\rho_{Nc}(T, x)$ results represent inter-layer transport. In the anisotropic cuprates, a prevalent model for the transport mechanisms assumes a strong in-plane coupling where superconductivity occurs, and a weak-link, Josephson coupling between the planes. One such model was discussed by Graf, Rainer and Sauls[29], where the normal c-axis, inter-layer conductivity $\rho_{Nc} = 1/\rho_{Nc}$ is given by:

$$\sigma_{Nc} = 2N_f e^2 D \qquad (2)$$

where N_f is the density of states at the chemical potential. This allowed us to calculate the inter-layer diffusion constant D and the corresponding ξ_{Nd} of Eq. (1), using the measured resistivity values while the density of states values were taken from Ino et al[30]. Using this procedure, we calculated the ratio between the normal coherence lengths of the $x=0.18$ and $x=0.1$ Sr doped barriers. This yields $\frac{\xi_{Nd}(0.18)}{\xi_{Nd}(0.1)} \simeq 1.2 \pm 0.1$ at 60 K, which disagrees with the measured coherence lengths of Fig. 4 at this temperature. Generally, the diffusion constant D and therefore also ξ_N, should be larger in the less resistive materials, those with the higher doping level, as is actually seen in the low temperature regime of Fig. 4. The fact that this behavior is reversed at the high temperature regime, must be due to an unconventional proximity effect where the LSCO-0.1 barrier
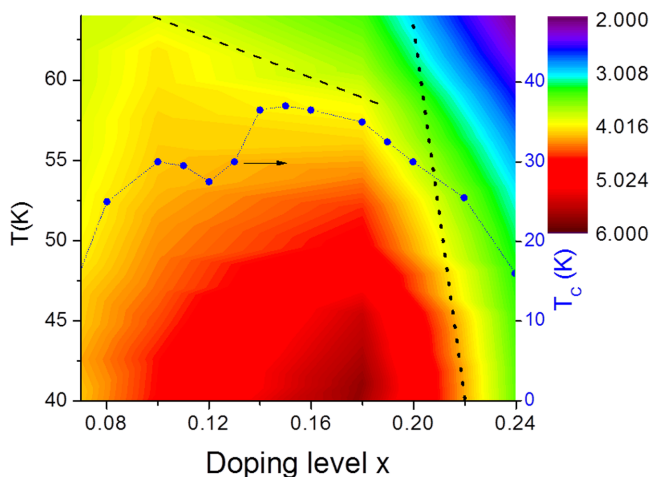
Figure 5 | A color-map of the phase diagram of $\xi_N(T, x)$ representing the normal coherence length of LSCO-x in nm as function of temperature T and doping x. The dotted line represents the pseudogap T* temperature of Ref. 32, while the dashed line describes the trend of the present data of ξ_N for $0.18 \geq x \geq 0.1$ and $T > 55$ K. For comparison we plot also $T_c(x)$ measured on LSCO single crystals by Matsuzaki et al.[36].

does not behave as a normal metal. Some feature of this barrier should facilitate the long range proximity effect and the preference for higher ξ_N values in the underdoped regime at higher temperatures. We attribute this behavior to the precursor superconductivity scenario, in which the conjectured uncorrelated pairs (preformed pairs) allow for these phenomena to occur.

The phase diagram of $\xi_N(T, x)$. To further elucidate and explain this interpretation of our results, we plot in Fig. 5 a color-map of the full phase diagram of $\xi_N(T, x)$. All the measured $\xi_N(T)$ values of the x=0.07, 0.1, 0.18 and 0.24 doping levels were used (12 × 4 measured values at 12 temperatures per each doping level), and the color-map extrapolates and draws the contours in between these doping levels. The contours in between the measured data points should thus be considered only as guides to the eye. We have data also below 40 K, but this is less reliable due to flux flow effects and we have chosen not to show it here. A clear feature in Fig. 5 is that the contours of constant ξ_N follow roughly the superconducting dome, but this occurs much above the T_c values of the LSCO-x barrier. Moreover, above 55 K, the maximum ξ_N values for each contour occurs at moderate under-doping (x=0.1). One can see this behavior also by looking at the dashed line which shows the general trend of the contours in the $0.1 < x < 0.18$ doping range at high temperatures. Although reminiscent of the pseudogap T* behavior as depicted from ARPES measurements by the dotted line[31], the slopes of the two lines are very different, possibly indicating the presence of additional effects such as phase fluctuations or that the two phenomena are unrelated[20,21]. Similar phase diagram trends were observed before in the cuprates in Nernst effect measurements[32], in high magnetic field results[33], in infrared and terahertz spectroscopy[17,34], and in higher energy gap results obtained in Andreev conductance spectroscopy measurements[35]. These previous results, as well as the new one presented here, provide additional support for strong superconducting fluctuation effects and the preformed pairs scenario in the underdoped regime of the cuprates above T_c but not necessarily up to the T* transition-line of the pseudogap.

In conclusion, comparative supercurrent measurements in SNS YBCO - LSCO-x - YBCO c-axis junctions at various temperatures and doping levels x, yielded a novel phase diagram of $\xi_N(T, x)$, which

besides the observation of a long range proximity effect, also support the precursor superconductivity scenario in the underdoped regime of the cuprates above T_c.

1. Timusk, T. & Statt, B. The pseudogap in high-temperature superconductors: an experimental survey. *Rep. Prog. Phys.* **62**, 61–122 (1999).
2. Fischer, O., Kugler, M., Maggio-Aprile, I., Berthod, C. & Renner, C. Scanning tunneling spectroscopy of high-temperature superconductors. *Rev. Mod. Phys.* **79**, 353–419 (2007).
3. Emery, V. J. & Kivelson, S. A. Importance of phase fluctuations in superconductors with small superfluid density. *Nature* **374**, 434–437 (1995).
4. Deutscher, G. Coherence and single-particle excitations in the high-temperature superconductors. *Nature* **397**, 410412 (1999).
5. Tanaka, K. *et al.* Distinct Fermi-momentum-dependent energy gaps in deeply underdoped Bi2212. *Science* **314**, 19101913 (2006).
6. Blanco-Canosa, S. *et al.* Momentum-Dependent Charge Correlations in $Y Ba_2Cu_3O_{6+\delta}$ Superconductors Probed by Resonant X-Ray Scattering: Evidence for Three Competing Phases. *Phys. Rev. Lett.* **110**, 187001 (2013).
7. LeBoeuf, D. *et al.* Thermodynamic phase diagram of static charge order in underdoped $Y Ba_2Cu_3O_y$. *Nat. Phys.* **9**, 79–83 (2013).
8. Fauque, B. *et al.* Magnetic order in the pseudogap phase of high-T_c superconductors. *Phys. Rev. Lett.* **96**, 197001 (2006).
9. Xia, J. *et al.* Polar Kerr-effect measurements of the high-temperature $Y Ba_2Cu_3O_{6+x}$ superconductor: Evidence for broken symmetry near the pseudogap temperature. *Phys. Rev. Lett.* **100**, 127002 (2008).
10. Hosur, P., Kapitulnik, A., Kivelson, S. A., Orenstein, J. & Raghu, S. Kerr effect as evidence of gyrotropic order in the cuprates. *Phys. Rev. B* **87**, 115116 (2013).
11. Lubashevsky, Y. *et al.* Optical Birefringence and Dichroism of Cuprate Superconductors in the THz regime. *Phys. Rev. Lett.* **112**, 147001 (2014).
12. Varma, C. M. Gyrotropic birefringence in the under-doped cuprates. EPL **106**, 27001 (2014). arXiv, 1310.8275 (2013).
13. Kanigel, A. *et al.* Evidence for pairing above the transition temperature of cuprate superconductors from the electronic dispersion in the pseudogap phase. *Phys. Rev. Lett.* **101**, 137002 (2008).
14. Shi, Ming. *et al.* Spectroscopic evidence for preformed Cooper pairs in the pseudogap phase of cuprates. *EPL* **88**, 27008 (2009).
15. Lee, W. S. *et al.* Abrupt onset of a second energy gap at the superconducting transition of underdoped Bi2212. *Nature* **450**, 81 (2007).
16. Boyer, M. C. *et al.* Imaging the two gaps of the high-temperature superconductor $Bi_2Sr_2CuO_{6+x}$. *Nat. Phys.* **3**, 802 (2007).
17. Dubroka, A. *et al.* Evidence of a precursor puperconducting phase at temperatures as high as 180 K in $RBa_2Cu_3O_{7−\delta}$ (R = Y, Gd, Eu) superconducting crystals from infrared spectroscopy. *Phys. Rev. Lett.* **106**, 047006 (2011).
18. Wu, Tao *et al.* Emergence of charge order from the vortex state of a high-temperature superconductor. *Nat. Commun.* **4**, 1–6 (2013).
19. Dong, T., Zhou, F. & Wang, N. L. *Phys. Rev. B* **88**, 184507 (2013).
20. Shekhter, A. *et al.* Bounding the pseudogap with a line of phase transitions in $Y Ba_2Cu_3O_{6+\delta}$. *Nature* **498**, 75–77 (2013).
21. Miller, J. L. Ultrasound measurements reveal a long-sought phase transition in superconducting cuprates. *Phys. Today* **66**, 12 (2013).
22. Bozovic, I. *et al.* Giant proximity effect in cuprate superconductors. *Phys. Rev. Lett.* **93**, 157002 (2004).
23. Bergeal, N. *et al.* Pairing fluctuations in the pseudogap state of copper-oxide superconductors probed by the Josephson effect. *Nat. Phys.* **4**, 608 (2008).
24. Covaci, L. & Marsiglio, F. Proximity effect and Josephson current in clean strong/weak/strong superconducting trilayers. *Phys. Rev. B* **73**, 014503 (2006).
25. Marchand, D., Covaci, L., Berciu, M. & Franz, M. Giant proximity effect in a phase-fluctuating superconductor. *Phys. Rev. Lett.* **101**, 097004 (2008).
26. Kirzhner, T. & Koren, G. Interface effects in d-wave superconductor-ferromagnet junctions in the vicinity of domain walls. *Phys. Rev. B* **82**, 134507 (2010).
27. Gross, R., Chaudhari, P., Dimos, D., Gupta, A. & Koren, G. Thermally activated phase slippage in High-T_c grain-boundary Josephson junctions. *Phys. Rev. Lett.* **64**, 228 (1990).
28. de Gennes, P. G. Boundary effects in superconductors. *Rev. Mod. Phys.* **36**, 225 (1964).
29. Graf, M. J., Rainer, D. & Sauls, J. A. Coupled two-dimensional Fermi liquids as a model for layered superconductors: Basic equations and elementary results. *Phys. Rev. B* **47**, 12089 (1993).
30. Ino, A., Mizokawa, T. *et al.* Doping dependent density of states and pseudogap behavior in $La_{2−x}Sr_xCuO_4$. *Phys. Rev. Lett.* **81**, 2124 (1998).
31. Yoshida, T. *et al.* Universal versus material-dependent two-gap behaviors of the high-Tc cuprate superconductors: Angle-resolved photoemission study of $La_{2−x}Sr_xCuO_4$. *Phys. Rev. Lett.* **103**, 037004 (2009).
32. Wang, Yayu., Li, Lu. & Ong, N. P. Nernst effect in high-T_c superconductors. *Phys. Rev. B* **73**, 024510 (2006).
33. Rullier-Albenque, F., Alloul, H. & Rikken, G. High-field studies of superconducting fluctuations in high-T_c cuprates: Evidence for a small gap distinct from the large pseudogap. *Phys. Rev. B* **84**, 014522 (2011).

34. Bilbro, L. S. *et al.* Temporal correlations of superconductivity above the transition temperature in $La_{2-x}Sr_xCuO_4$ probed by terahertz spectroscopy. *Nat. Phys.* **7**, 298 (2011).

35. Koren, G. & Kirzhner, T. Observation of two Andreev-like energy scales in $La_{2-x}Sr_xCuO_4$ superconductor/normal-metal/superconductor junctions. *Phys. Rev. Lett.* **106**, 017002 (2011).

36. Matsuzaki, T. *et al.* Superconducting gap and pseudogap behavior in high-T cuprates. *Phys Chem Sol* **62**, 29–33 (2001).

Acknowledgments

Author contributions

T.K. had initiated this project and made the major part of the experiments. G.K. made some of the experiments and both have written this manuscript.

Additional information